Dimensionality dependence of mode-locking dynamics in charge-density-wave transport

J. McCarten,* D. A. DiCarlo, and R. E. Thorne
Laboratory of Atomic and Solid State Physics and Materials Science Center, Cornell University, Ithaca, New York 14853
(Received 15 March 1993; revised manuscript received 27 September 1993)

We estimate the widths of the harmonic mode-locked steps observed on the dc *I-V* characteristic of charge-density-wave (CDW) conductors when ac and dc voltages are applied together using the classical deformable medium model. For weakly pinned CDW's in the high-velocity limit, $\delta E_{p/1}/E_T = 2|J_p(\omega_{c0}E_{ac}/\omega_{ac}E_T)|^{4/(4-D)}$ where $\delta E_{p/1}$ is the width in electric field of the $p/1$ step and D is the effective dimension of the pinning. An analytic argument suggests that the phase deformations are much larger in the mode-locked state than in the normal sliding state. They are largest for ac amplitudes that yield maxima in the step width. On the $p/1$ step the time-averaged phase-phase correlation length is predicted to vary as $\delta E_{p/1}^{-1/2}$. These analytic estimates are supported by numerical simulations. Measurements of the step width variation with ac amplitude and frequency for $NbSe_3$ crystals whose static pinning is two dimensional (2D) are consistent with the 2D step width prediction.

I. INTRODUCTION

Motion of charge-density waves (CDW's) in compounds like $NbSe_3$, TaS_3, $K_{0.3}$, MoO_3, and $(TaSe_4)_2I$ results in several unusual electrical transport effects.[1] These include nonlinear dc conduction above a threshold field E_T,[2,3] strongly frequency-dependent ac conduction,[4] coherent voltage oscillations (narrow-band noise) in response to dc electric fields,[3] and mode-locking phenomena in response to combined ac and dc fields.[5,6] These effects result from the interaction between the CDW and impurities (or other defects) which destroy the translational invariance of the CDW and pin it to the lattice. Two types of pinning are distinguished:[7-9] (i) strong pinning, in which the CDW phase is pinned at each impurity site so that the CDW phase-phase correlation length (l_{ph}) is just the average spacing between impurities, and (ii) weak pinning, in which fluctuations in the random impurities potential pin the CDW on much longer length scales.

Recent experiments have established that CDW's in $NbSe_3$ are weakly pinned, and that the bulk phase-phase correlation length in undoped crystals is much larger than the thickness (t) of typical crystals.[10,11] Since reduced dimensionality is imposed if one or more sample dimensions are less than the bulk l_{ph} value, most crystals are in the confined two-dimensional (2D) limit for static pinning.

Here we investigate the effects of pinning dimensionality on mode-locking dynamics in the sliding CDW state. We estimate the harmonic step width dependence on ac amplitude and dimensionality using the classical deformable medium model (CDMM). These estimates are obtained by combining the mode-locking argument for the single coordinate model (SCM) introduced by Shapiro, Janus, and Holly to describe Josephson junctions[12] with weak pinning scaling arguments introduced by Imry and Ma,[13] and are consistent with the results of numerical simulations. We show that the 2D estimate is consistent with experimental data for $NbSe_3$ samples whose static pinning is 2D. We also describe analytical and numerical calculations which yield insight into the nature of CDW phase correlations in the mode-locked state.

II. REVIEW OF PREVIOUS WORK

When a voltage $V(t)=V_{dc}+V_{ac}\cos(\omega_{ac}t)$ is applied to a CDW crystal, the dc *I-V* characteristic exhibits steps where the dc CDW current remains constant while the dc voltage varies.[5] These steps are due to mode locking of the internal CDW frequency associated with dc flow $\omega_1/2\pi$ with the applied ac frequency $\omega_{ac}/2\pi$. Both harmonic steps, for which $\omega_1/\omega_{ac}=p$, and subharmonic steps, for which $\omega_1/\omega_{ac}=p/q$, are observed. The internal frequency ω_1 results because the CDW pinning is periodic with respect to integral displacements of CDW wavelengths. When ω_{ac} is near a rational multiple of ω_1, the periodic CDW-impurity interaction produces an additional time-averaged pinning force which adds to the applied dc electric-field force. The step width δV is proportional to the maximum of this time-averaged pinning force, and thus provides information about the CDW-impurity interaction in a dynamic limit.

Previous investigators[14-16] have shown that some qualitative features of mode locking in $NbSe_3$ are described by an overdamped SCM with a sinusoidal pinning potential,

$$\gamma\dot{\phi}=\frac{e\rho_{eff}}{Q}[E-E_T\sin(\phi)]\ , \tag{1}$$

where $\dot{\phi}$ is proportional to the CDW current.[17] This model is analogous to the resistively shunted junction model for Josephson junctions with I and V exchanged. Early measurements[14-16] on poor-quality $NbSe_3$ crystals that did not show complete locking were reported to yield step width oscillations which agreed qualitatively and quantitatively with the SCM predictions. Subsequent measurements[18-20] indicated that oscillations could not be observed in samples of the quality used in Refs. [14-16], and that in extremely high-quality crystals[18,19] the oscillations differed qualitatively and quantitatively

from the SCM predictions. In particular, the predicted maximum value of the harmonic step widths and predicted shape of the step width oscillations with ac amplitude were all inconsistent with experiment. Furthermore, the SCM predicts subharmonic steps only if the pinning potential is nonsinusoidal.

Extensive theoretical efforts have been made to understand how spatial degrees of freedom influence mode-locking behavior.[21-24] Numerical simulations of the CDMM have found complete locking in large systems and have reproduced many of the salient features of the experimental data.[23-25] In an analytic treatment of mode locking within this model, Matsukawa and Takayoma found that a standard perturbation expansion breaks down near where the mode-locked steps are expected to occur. Assuming the size of this region is proportional to the width of the 1/1 step, $\delta E_{1/1}$, he showed that to first order $\delta E_{1/1} \propto |J_1(\omega_{co}E_T/\omega_{ac}E_T)|^{4/(4-D)}$ for weak pinning in the high velocity ($E_{dc} \gg E_T$) limit.[26]

III. ANALYTIC ESTIMATE

The CDW state is typically described by a complex order parameter $\Psi=\Delta e^{i\phi}$, where Δ is proportional to the amplitude of the lattice distortion and ϕ is the phase (position) of the distortion within the crystal. The CDMM assumes amplitude distortions are of high enough energy so that can be neglected. The equation of motion in the overdamped limit then reduces to[7-9,21,26]

$$\tilde{\gamma}\frac{\partial\phi}{\partial t}=\frac{e\tilde{\rho}_{\rm eff}}{Q}E+F_P[x,\phi(x,t)] , \tag{2}$$

where $\tilde{\gamma}$ is a phenomenological damping constant, $e\tilde{\rho}_{\rm eff}$ the effective CDW charge density, E is the electric field along the CDW chain axis, and Q is the CDW wave vector. The pinning force is given by

$$F_P[x,\phi(x,t)]=-\frac{\delta}{\delta\phi}H_{\rm pin}[x,\phi(x,t)] , \tag{3}$$

where

$$H_{\rm pin}[x,\phi(x,t)]=\int\frac{\tilde{f}}{2}(\Delta\phi)^2d^Dx + \sum_i^{N_{\rm imp}} v\rho_1\cos[Qx_i+\phi(x_i,t)] . \tag{4}$$

Here $\tilde{f}$ represents the CDW strain coefficient and $v\rho_1$ the magnitude of the pinning potential for an individual impurity. The short-range interaction of an individual impurity has been approximated by a delta function. The sum $\sum_i^{N_{\rm imp}}$ is over a random distribution of impurities of concentration $\tilde{n}_i$. Length scales have been rescaled to make the phase-phase correlation lengths isotropic.[27] In this model, the CDW current is just proportional to $(\partial\phi/\partial t)_x$ where $(\ )_x$ indicates a spatial average.

The weak pinning limit in this model occurs when the dimensionless pinning parameter,

$$\varepsilon_i=\frac{v\rho_1}{\tilde{f}\tilde{n}_i^{-1+2/D}} , \tag{5}$$

which is the ratio of the characteristic pinning energy per impurity to the characteristic elastic energy per impurity, is much less than 1. In this limit fluctuations in the random impurity pinning potential pin the CDW on a length scale $l_{\rm ph} \propto n_i^{1/(D-4)}$ if $D<4$ and $E_T \propto p_{\rm ph}^{-2}$.

Here we will proceed to estimate the width of the harmonic mode-locked steps in the weak-pinning limit. Instead of using perturbation theory, we will follow a more intuitive approach based on that due to Shapiro for the SCM model [Eq. (1)]. We consider the case where the CDW is biased with a superposition of a dc and ac current, $(\partial\phi(x,t)/\partial t)_x=-\omega_1+\omega_{\rm amp}\cos(\omega_{\rm ac}t)$. Then

$$\phi(x,t)=-\omega_1 t+\frac{\omega_{\rm amp}}{\omega_{\rm ac}}\cos(\omega_{\rm ac}t)+\delta\phi(x,t) , \tag{6}$$

where $\langle\partial\delta\phi(x,t)/\partial t\rangle_x=0$. Substituting Eq. (6) into (4) yields

$$H_{\rm pin}[x,\phi(x,t)]=\int\frac{\tilde{f}}{2}(\nabla\delta\phi)^2d^Dx+\sum_i^{N_{\rm imp}}\sum_{p=-\infty}^{+\infty} v\rho_1 J_p\left[\frac{w_{\rm amp}}{\omega_{\rm ac}}\right]\cos[Qx_i+\delta\phi(x_i,t)+(p\omega_{\rm ac}-\omega_1)t] . \tag{7}$$

The mode-locked state is assumed to occur when the time-averaged pinning energy in the locked state is lower than in the unlocked state. On the harmonic steps the CDW advances an integral number of wavelengths per ac cycle so the dominant contribution to the time-averaged pinning energy arises from the time-independent part of $\delta\phi(x,t)$. Assuming $\delta\phi(x,t)=\delta\phi(x)$, Eq. (7) reduces to

$$\langle H_{\rm pin}[x,\phi(x)]\rangle_t=\int\frac{\tilde{f}}{2}(\nabla\delta\phi)^2d^Dx\sum_i^{N_{\rm imp}}\sum_{p\omega_{\rm ac}=\omega_1} v\rho_1 J_p\left[\frac{\omega_{\rm amp}}{\omega_{\rm ac}}\right]\cos[Qx_i+\delta\phi(x_i)] . \tag{8}$$

Thus, in analogy with the argument of Shapiro, Janus, and Holly, the time-averaged pinning energy to depend on the particular configuration $\delta\phi(\bar{x})$. For some range of configurations, the CDW pinning energy will be less than in the unlocked state. Through variations over this range the time-averaged pinning force can adjust itself to cancel changes in the dc electric field, so as to keep the total time-averaged force on the CDW, and thus the dc CDW current, constant.

In the weak-pinning limit, scaling arguments can be used to estimate the maximum magnitude of the time-averaged pinning energy.[13] Equations (4) and (8) indicate

that the pinning Hamiltonian or the static case and the time-averaged Hamiltonian for the harmonic mode-locked case are identical, except that the individual impurity pinning strength in the static case, $v\rho_1$, is replaced by $J_p(\omega_{\rm amp}/\omega_{\rm ac})v\rho_1$ on the $p/1$ step. Assuming the angle through which the CDW must be polarized before depinning is the same for the static case and the $p/1$ step yields

$$\frac{\delta E_{p/1}}{E_T}=2\left|J_p\left[\frac{\omega_{\rm amp}}{\omega_{\rm ac}}\right]\right|^{4/(4-D)}, \tag{9}$$

where D represents the "effective" pinning dimension of the sample. For $D=0$, the SCM result is recovered. In the high velocity limit $E_{\rm dc}\gg E_T$, $\omega_{\rm amp}/\omega_{\rm co}\approx E_{\rm ac}/E_T$, and the Bessel function argument reduces to $\omega_{\rm co}E_{\rm ac}/\omega_{\rm ac}E_T$.[28] This result is thus consistent with Matsukawa's perturbation analysis that was discussed in Sec. II (Ref. 26) except here we have also estimated the numerical prefactor.

IV. 1D NUMERICAL SIMULATIONS

To investigate the range of validity of Eq. (9), 1D numerical simulations were performed. $\tilde{\gamma}$ was set equal to unity and the lattice was discretized by the same procedure used by Matsukawa and Takayama.[26] The equation of motion was developed using the alternating-direction-implicit method[29,30] and cyclic-boundary conditions were imposed on the lattice.

Great care must be taken to ensure that simulations of weak-pinning dynamics are not finite size limited. The static phase-phase correlation length gives a rough estimate of the cross over from bulk to finite size behavior. If the sample size l is much less than $l_{\rm ph}$ the dynamics will be in the $D=0$ (SCM) limit. Matsukawa and Takayama estimate that[26]

$$l_{\rm ph}\approx\left[\frac{3}{2\pi^2}\varepsilon_i\right]^{2/(D-4)}\tilde{n}_i^{-1/D}. \tag{10}$$

This presents a problem. To study weak-pinning dynamics, $\varepsilon_i\ll 1$, but this makes $l_{\rm ph}$ large so very large simulations are required. However, increasing ε_i to reduce $l_{\rm ph}$ may contaminate the dynamics with strong-pinning corrections.

For $1D$ self-consistency checks were performed to determine the bulk limit solution for the width of the 1/1 step in the weak-pinning limit. We began the 1D simulations with $\varepsilon_i=1$ and 128 lattice sites and found the $\delta E_{1/1}-E_{\rm ac}$ curve to fall between the $D=0$ and $D=1$ predictions of Eq. (9). Simulations were then performed with $\varepsilon_i=\frac{1}{2}$, $\frac{1}{4}$, and $\frac{1}{8}$. The $\delta E_{1/1}-E_{\rm ac}$ curves converged toward the $D=1$ prediction with decreasing ε_i, and the $\varepsilon_i=\frac{1}{4}$ and $\varepsilon_i\frac{1}{8}$ results were almost identical. Simulations of various lattice sizes with $\varepsilon_i=\frac{1}{8}$ were then performed to distinguish between the bulk and finite size limits.

Figure 1 shows $\delta E_{1/1}/E_T$ versus $\omega_{\rm co}E_{\rm ac}/\omega_{\rm ac}E_T$ for three 1D simulations with lattice sizes $l=8$, 128, and 512. Here $\varepsilon_i=\frac{1}{8}$, $n_i=1$, and $\omega_{\rm ac}=12\omega_{\rm co}$. As expected the $l=8$ lattice reproduces the $D=0$ SCM result since $l_{\rm ph}\approx 14$. For $l=128$ and 512, Eq. (9) for $D=1$ gives a more accurate fit to the numerical data. Coefficients extracted from $l=512$ data using a fit $\delta E_{1/1}/E_T=a|J_1(b\omega_{\rm co}E_{\rm ac}/\omega_{\rm ac}E_T)|^c$ are $a=2.1\pm0.1$, $b=0.99\pm0.02$, and $c=1.39\pm0.05$ in good agreement with Eq. (9).

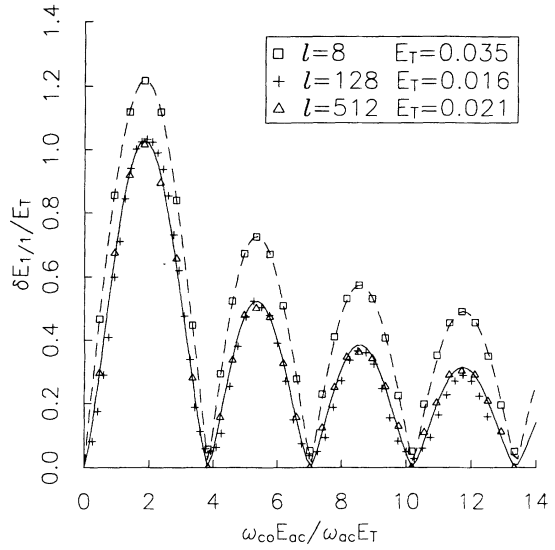

FIG. 1. $\delta E_{1/1}/E_T$ vs $\omega_{\rm co}E_{\rm ac}/\omega_{ac}E_T$ for 1D numerical simulations with 8, 128, and 512 lattice sites. For the simulations $\varepsilon_i=\frac{1}{8}$, $n_i=1$, and $\omega_{\rm ac}=12\omega_{\rm co}$. Dashed and solid lines give the best fits of $a|J_1(b\omega_{\rm co}E_{\rm ac}/\omega_{\rm ac}E_T)|^c$ to the $l=8$ and 512 data, respectively. For $l=8$, $a=2.1$, $b=1.00$, and $c=0.99$ and for $l=512$, $a=2.1$, $b=1.00$, and $c=1.39$, in good agreement with the $D=0$ and 1 fits of Eq. (9).

Figure 2 shows $\delta E_{2/1}/E_T$ versus $\omega_{\rm co}E_{\rm ac}/\omega_{\rm ac}E_T$ for 1D

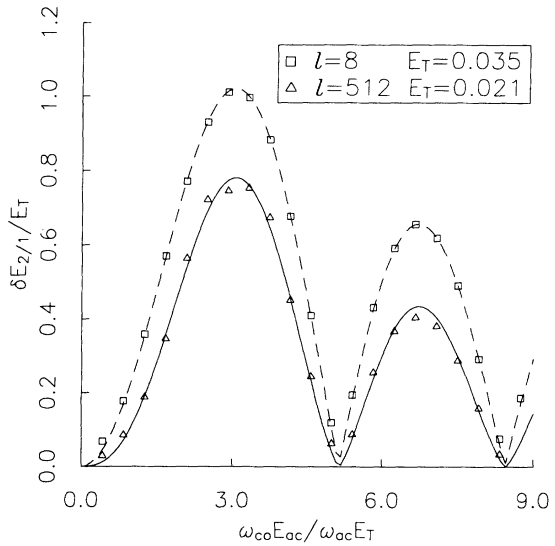

FIG. 2. $\delta E_{2/1}/E_T$ vs $\omega_{\rm co}E_{\rm ac}/\omega_{\rm ac}E_T$ for 1D numerical simulations with 8 and 512 lattice sites. For the simulations $\varepsilon_i=\frac{1}{8}$, $n_i=1$, and $\omega_{\rm ac}=12\omega_{\rm co}$. Dashed and solid lines give the best fits of $a|J_2(b\omega_{\rm co}E_{\rm ac}/\omega_{\rm ac}E_T)|^c$ to the $l=8$ and 512 data, respectively. For $l=8$, $a=2.1$, $b=1.00$, and $c=1.00$ and for $l=512$, $a=2.05$, $b=1.00$, and $c=1.33$, in good agreement with the $D=0$ and 1 fits of Eq. (9).

simulations of $l=8$ and 512, using the same parameter values as in Fig. 1. Coefficients extracted from the arbitrary fit $a|J_2(b\omega_{co}E_{ac}/\omega_{ac}E_T)|^c$ are $a=2.1\pm0.1$, $b=1.00\pm0.02$, and $c=1.00\pm0.01$ for $l=8$ and $a=2.05\pm0.1$, $b=1.00\pm0.02$, and $c=1.33\pm0.01$ for $l=512$, consistent with the $D=0$ and $D=1$ predictions, respectively.

The good agreement between the 1D numerical simulations and Eq. (9) suggests that the basic ideas involved in the analytic estimate of Sec. III are valid and can be extended to gain insight into the spatial structure of the CDW phase on the mode-locked steps. Equation (8) suggests that the ac field "effectively" renormalizes the magnetiude of the individual impurity pinning strength. Thus, many of the ideas used to describe the $E<E_T$ pinned state in the absence of an ac field can be extended to the mode-locked state. On the 1/1 step the pinning parameter in the high-field limit is effectively

$$\varepsilon_i^{1/1}=\frac{J_1\left(\dfrac{\omega_{co}E_{ac}}{\omega_{ac}E_T}\right)v\rho_1}{\tilde{f}\tilde{n}_i^{-1+2/D}} . \tag{11}$$

From Eq. (10), the "effective" time-averaged phase-phase correlation length on the step $l_{ph}^{1/1}$ will be greater for E_{ac} values that give smaller J_1 values. Furthermore, since $|J_1(x)|<1$ for all values of x, $l_{ph}^{1/1}$ will always be greater than the static phase-phase correlation length.

1D simulations were performed to investigate the ac amplitude dependence of $l_{ph}^{1/1}$. To help evaluate these results, simulations of the $E_{ac}=0$ sliding and pinned states were performed. Figure 3 shows the time and space-averaged correlation function $([\phi(n)-\phi(0)]^2)$ versus n for four different E_{dc} values greater than E_I. Here n represents the distance between discretized lattice sites. The time-averaged phase deformations decrease with increasing velocity; for $E_{dc}>25E_T$ the time-averaged phase deformations are practically undetectable implying a sample-size limited phase-phase correlation length.

Below threshold we observed that after the CDW was depinned and then repinned there was some hysteresis in the static phase configuration but little change in $([\phi(n)-\phi(0)]^2)$ as E_{dc} was scanned between $-E_T$ and E_T.[31] This is consistent with numerical simulations performed by Middleton and Fisher, and their description of the CDW polarizations below E_T.[32]

Application of an ac electric field has dramatic effects on the spatial structure of the phase. In the high-velocity limit, we find that as the 1/1 step is approached, the phase deformations is increase substantially. Figure 4 shows $\langle[\phi(n)-\phi(0)]^2\rangle$ versus n for four different dc electric fields near the 1/1 step. Here E_{ac} is such that the width of the 1/1 step is at its first maximum.

On the 1/1 step, we find that $\langle[\phi(n)-\phi(0)]^2\rangle$ does not change significantly as E_{dc} is varied. $l_{ph}^{1/1}$ values extracted from the fit

$$\langle[\phi(n)-\phi(0)]^2\rangle=(n/l_{ph}^{1/1})^2 \tag{12}$$

for $n<50$ varied by $\pm10\%$ as E_{dc} was scanned between the high- and low-field sides of the locked region.[31] We did observe a small amount of hysteresis on the step, consistent with previous observations by Middletown.[33] Figure 5 shows typical $\langle[\phi(n)-\phi(0)]^2\rangle$ data on the 1/1 step versus n for E_{ac} values between the first width maximum and the first width node of the 1/1 step. At the first node, the CDW remains unlocked for all dc electric field values and the phase is advancing with almost no spatial distortions. As the step width increases the phase deformations also increase. To analyze the length scale divergence at the node, $l_{ph}^{1/1}$ was calculated for each E_{ac} value

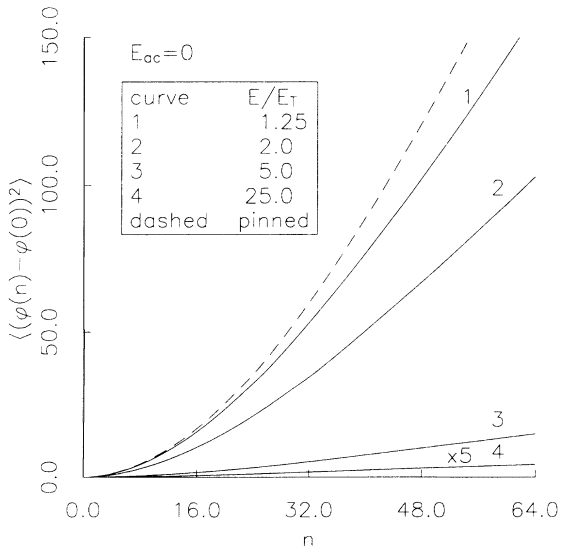

FIG. 3. $\langle[\phi(n)-\phi(0)]^2\rangle$ vs lattice separation n at several dc fields for $E_{ac}=0$. For these 1D simulations, $\varepsilon_i=\frac{1}{8}$, $n_i=1$, $l=512$, and $\omega_{ac}=12\omega_{co}$. The dashed line shows $\langle[\phi(n)-\phi(0)]^2\rangle$ for $E_{dc}=0$ after the CDW had been depinned and then repinned.

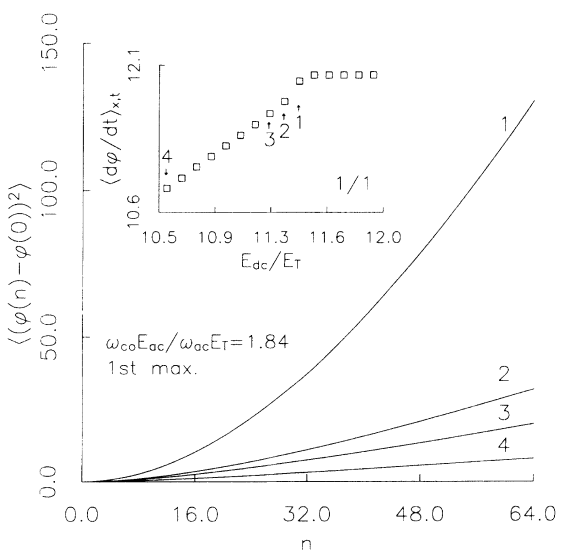

FIG. 4. $\langle[\phi(n)-\phi(0)]\rangle$ vs lattice separation n for different E_{dc} values approaching the 1/1 step (at the first step width maximum) from the low-field side. Similar behavior is observed on the high-field side. Simulation parameters were $\varepsilon_i=\frac{1}{8}$, $n_i=1$, $l=512$, and $\omega_{ac}=12\omega_{co}$.

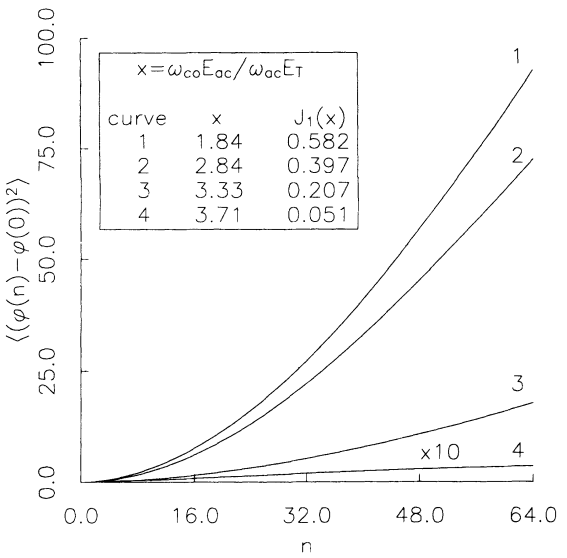

FIG. 5. Typical $\langle[\phi(n)-\phi(0)]^2\rangle$ data on the 1/1 step vs lattice separation n for four different E_{ac} values. For the 1D simulations, $\varepsilon_i=\frac{1}{8}$, $n_i=1$, $l=512$, and $\omega_{ac}=12\omega_{co}$ and $E_T=0.021$. As $J_1(\omega_{ac}E_{ac}/\omega_{co}E_T)\rightarrow 0$, the time-averaged phase-phase correlations grow and eventually exceed the size of the lattice.

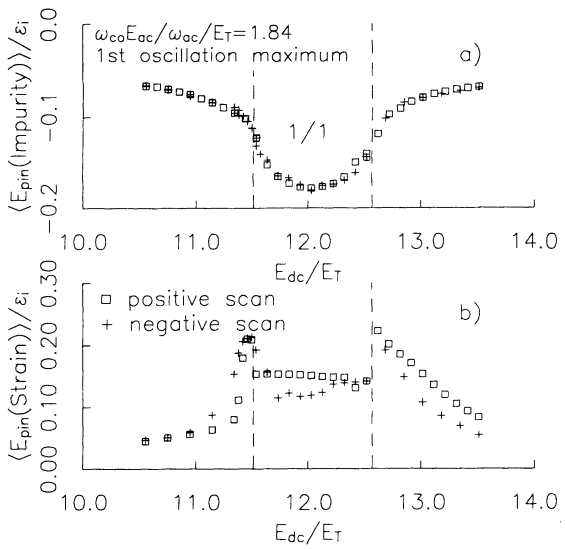

FIG. 6. 1D numerical results for (a) the time- and space-averaged impurity pinning energy $\langle E_{pin}^{imp}\rangle$ and (b) the time- and space-averaged elastic energy $\langle E_{pin}^{str}\rangle$ vs dc electric field at the first maximum of the 1/1 step width. For the simulation $\varepsilon_i=\frac{1}{8}$, $n_i=1$, $l=512$, and $\omega_{ac}=12\omega_{co}$. On the step $\langle E_{pin}^{str}\rangle$ displays hysteresis while $\langle E_{pin}^{imp}\rangle$ does not. The multiplicity of $\langle E_{pin}^{str}\rangle$ on the high- and low-field sides of the 1/1 step is due to the finite length of the time average (100 transient cycles and 100 averaged cycles).

using Eq. (12). We find

$$l_{ph}^{1/1}\propto|J_1(\omega_{co}E_{ac}/\omega_{ac}E_T)|^{-c},$$

where $c=0.6\pm0.15$. The uncertainty in the exponent primarily arises from the small amount of hysteresis on the mode-locked step. From Eqs. (10) and (11), the predicted exponent in 1D is $\frac{2}{3}$, consistent with the numerical result.

To gain further insight into the mode-locking dynamics, we also investigated the change in time-averaged impurity pinning energy per lattice site ($\langle E_{pin}^{imp}\rangle$) and time-averaged elastic energy per lattice site ($\langle E_{pin}^{str}\rangle$) on and near the 1/1 step. Figure 6 shows results for $\langle E_{pin}^{imp}\rangle$ and $\langle E_{pin}^{str}\rangle$ for the E_{ac} value where the width of the 1/1 step is at its first maximum. It is interesting to note that $\langle E_{pin}^{str}\rangle$ is discontinuous at the step edges and shows significant hysteresis on the step while $\langle E_{pin}^{imp}\rangle$ is continuous and smooth at the step edges and exhibits no perceptible hysteresis. The nonanalytical behavior of $\langle E_{pin}^{str}\rangle$ indicates that spatial strains and not the impurity restoring force control the mode-locked depinning and, therefore, the dynamic critical behavior. This behavior is notably different than the SCM where the time-averaged pinning energy of the sinusoidal potential possess a discontinuous derivative at the step edges.[30]

V. EXPERIMENTAL COMPARISON

We have attempted to test these mode-locking predictions through measurements on undoped $NbSe_3$ crystals. Transport[10] and x-ray[11] measurements have determined that the static phase-phase correlation length in the bulk limit along the thickness (a^*) direction is approximately 3–6 μm for the upper and lower transitions, respectively, for undoped $NbSe_3$ [$\rho(300\text{ K})/\rho(4.2\text{ K})\approx 300$]. All measured crystals reported here had thicknesses that were well into the limit for confined 2D static pinning.

Figure 7 shows $\delta E_{1/1}/E_T$ versus ac amplitude for $\omega_{ac}/2\pi=60$ MHz at $T=120$ K, the temperature where the quality of the mode locking is highest. For this sample, the mode-locking was complete on the 1/1 and 1/2

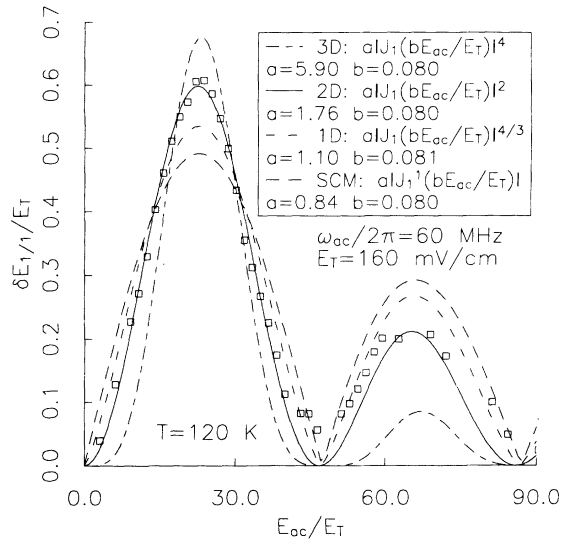

FIG. 7. The 1/1 step width $\delta E_{1/1}$, normalized by the $E_{ac}=0$ threshold field, $\delta E_{1/1}/E_T$, vs E_{ac}/E_T for an undoped $NbSe_3$ crystal that mode locked completely on the 1/1, 1/2, 1/3, and 2/3 steps. Sample dimensions are $l=0.50$ mm, $A=0.9$ μm^2, and $t=0.9$ μm. Fits are discussed in text.

steps, and subharmonics down the the $p/q=1/15$ could be resolved, indicating good velocity coherence. The best fit to the functional form $a|J_1(bE_{ac}/E_T)|^c$ with $c=2$ yields $a=1.76$, near the predicted value of 2 for 2D weak pinning. Driving the CDW at a higher frequency $\omega_{ac}=120$ MHz yields $a=1.9$.[34] A 1D fit with a power law of $c=\frac{4}{3}$ also describes the data fairly well, although the extracted prefactor $a=1.1$ is almost 50% smaller than the predicted value of 2. Two other very coherent samples gave nearly identical results for the upper transition.

We also took data on two samples near $T=50$ K, the temperature where the mode-locking quality is highest for the lower transition CDW. The best fit to the data in the high-velocity limit ($\omega_{ac}/2\pi>30$ MHz) to the functional form $a|J_1(bE_{ac}/E_T)|^2$ yields $a=1.9$ for both samples, again consistent with the 2D analytic estimate.

The analytic estimates and the numerical simulations presented in Secs. III and IV indicate that the mode-locking dynamics are sensitive to the dimensionality of the pinning in the weak limit. Our predictions for the functional form of the width of the $p/1$ step and for the functional form of the time-average phase-phase correlation length on the $p/1$ step versus ac electric-field amplitude and frequency are consistent with 1D numerical simulations. Larger simulations (which are beyond the scope of our computing power) are still needed to investigate the range of validity for the 2D and 3D predictions and to explore the nature of the 2D and 3D crossover.

The present experimental results indicate that the dimensionality dependence of the pinning must be accounted for when interpreting mode-locking data. The success of the 2D fit of Eq. (9) and $\delta E_{1/1}^{\max}$ scaling with E_T Ref. (10) indicates the mode-locking dynamics are 2D for most undoped $NbSe_3$ crystals. A complete test of the theory would involve measuring samples in the 1D and 3D limits. Obtaining samples in either of these two limits is extremely difficult. Large specimens almost always possess numerous thickness steps, giving a sample many CDW drift velocities[35] which makes data analysis difficult. Samples whose widths are small enough such that the crystal is in the 1D limit would be difficult to see optically. Also, thermal fluctuations become increasingly important with decreasing cross sectional area, altering the $T=0$ CDMM analysis.[36] Hopefully, improved sample preparation techniques will allow investigation of one or both of these two limits in the near future.

ACKNOWLEDGMENTS

We wish to thank H. Matsukawa, A. Middleton, and M. Kvale for fruitful discussions. Special thanks goes to S. Teulkosky for his help with our numerical simulations. Support was provided by the Cornell Physics/IBM joint study, administered by the Cornell Materials Science Center. Funding was provided by the Alfred P. Sloan Foundation, by the AT&T foundation, and by NSF Grant No. DMR-89-58515.

*Present address: Physics Department, UCLA, 405 Hilgard Ave., Los Angeles, CA 90024.

[1]For comprehensive reviews of CDW's, see P. Monceau, *Electronic Properties of Quasi-One-Dimensional Materials* (Reidel, Dordrecht, 1985), Pt. II, p. 139; G. Grüner, Rev. Mod. Phys. **60**, 1129 (1988).

[2]P. Monceau, N. P. Ong, A. M. Portis, A. Meerschaut, and J. Rouxel, Phys. Rev. Lett. **37**, 602 (1976).

[3]R. M. Fleming and C. C. Grimes, Phys. Lett. **42**, 1423 (1979).

[4]G. Grüner, A. Zettl, W. G. Clark, and J. Bardeen, Phys. Rev. B **24**, 7247 (1981).

[5]P. Monceau, J. Richard, and M. Renard, Phys. Rev. Lett. **45**, 43 (1980).

[6]J. Richard, P. Monceau, and M. Renard, Phys. Rev. B **25**, 948 (1982).

[7]H. Fukuyama, J. Phys. Soc. Jpn. **41**, 513 (1976).

[8]H. Fukuyama and P. A. Lee, Phys. Rev. B **17**, 535 (1978).

[9]P. A. Lee and T. M. Rice, Phys. Rev. B **19**, 3970 (1979).

[10]J. McCarten, D. DiCarlo, M. Maher, T. Adelman, and R. Thorne, Phys. Rev. B **46**, 4456 (1992).

[11]E. Sweetland, C-Y. Tsai, B. A. Winter, J. D. Brock, and R. E. Thorne, Phys. Rev. Lett. **65**, 3168 (1990).

[12]S. Shapiro, A. Janus, and S. Holly, Rev. Mod. Phys. **36**, 223 (1964).

[13]Y. Imry and S. Ma, Phys. Rev. Lett. **35**, 1399 (1975).

[14]G. Grüner, A. Zawadowski, and P. Chaikin, Phys. Rev. Lett. **46**, 511 (1981).

[15]P. Monceau, J. Richard, and M. Renard, Phys. Rev. B **25**, 931 (1982).

[16]A. Zettl and G. Grüner, Phys. Rev. B **29**, 755 (1984).

[17]For solution of Eq. (1), see J. Waldram and P. H. Wu, J. Low. Temp. Phys. **47**, 363 (1982).

[18]Y. Latyshev, V. Minakov, and Y. Rzhanov, Pis'ma Zh. Eksp. Teor. Fiz. **46**, 31 (1987) [JETP Lett. **46**, 37 (1987)].

[19]R. Thorne, W. Lyons, J. Tucker, and J. Bardeen, Phys. Rev. B **35**, 6360 (1987); R. Thorne, J. Hubacek, W. Lyons, J. Lyding, and J. Tucker, *ibid.* **37**, 10055 (1988).

[20]R. Thorne, J. R. Tucker, J. Bardeen, S. E. Brown, and G. Grüner, Phys. Rev. B **33**, 7342 (1986).

[21]L. Sneddon, M. Cross, and D. Fisher, Phys. Rev. Lett. **49**, 292 (1982).

[22]S. Coppersmith and P. Littlewood, Phys. Rev. Lett. **57**, 1927 (1986).

[23]H. Matsukawa, Synth. Met. **29**, F343 (1989).

[24]A. Middleton, O. Biham, P. Littlewood, and P. Sibani (unpublished).

[25]P. F. Tua and J. Ruvalds, Solid State Commun. **54**, 471 (1985).

[26]H. Matsukawa and H. Takayama, J. Phys. Soc. Jpn. **56**, 1507 (1987); H. Matsukawa, *ibid.* **56**, 1522 (1987); **57**, 3463 (1988).

[27]Parameters signified by a tilde are in the rescaled system.

[28]For this CDMM analysis, ω_{co} is defined to be $e\tilde{\rho}_{eff}E_T/\tilde{\gamma}Q$ and not the frequency where the imaginary part of the conductivity is a maximum.

[29]B. P. Flannery, S. A. Teukolsky, and W. T. Vetterling, *Numerical Recipes* (W. H. Press, Cambridge, 1987), p. 660.

[30]J. McCarten, Ph.D. thesis, Cornell University, Ithaca, New York, 1992.

[31]Changes in $\langle[\phi(n)-\phi(0)]^2\rangle$ within 5% of E_T or 3% of the mode-locked depinning were not investigated thoroughly.

[32]A. Middleton and D. Fisher, Phys. Rev. B **47**, 3530 (1993).

[33]A. Middleton (private communication).

[34]At 120 MHz, Ohmic heating distorts the I-V characteristic for E_{ac} values greater than those which give the first node in the Bessel-like oscillation. Two oscillations are measurable before Ohmic heating becomes a problem at 60 MHz. This is why the 60-MHz data instead of the 120-MHz data is shown in Fig. 7.

[35]M. Maher, T. Adelman, J. McCarten, D. DiCarlo, and R. Thorpe, Phys. Rev. B **43**, 9968 (1991).

[36]J. McCarten, M. Maher, T. Adelman, D. DiCarlo, and R. Thorne, Phys. Rev. B **43**, 6800 (1991).